JOURNAL OF MATERIALS SCIENCE 30 (1995) 661–677

Tensile creep behaviour of a silicon carbide-based fibre with a low oxygen content

R. BODET*, X. BOURRAT, J. LAMON, R. NASLAIN
Laboratoire des Composites Thermostructuraux (UMR 47 CNRS-SEP-UB1), Domaine Universitaire, 3, Allée de la Boëtie, 33600 Pessac, France

The high-temperature mechanical behaviour and microstructural evolution of experimental SiC fibres (Hi-Nicalon) with a low oxygen content (<0.5 wt%) have been examined up to 1600 °C. Comparisons have been made with a commercial Si–C–O fibre (Nicalon Ceramic Grade). Their initial microstructure consists of β-SiC crystallites averaging 5–10 nm in diameter, with important amounts of graphitic carbon into wrinkled sheet structures of very small sizes between the SiC grains. The fall in strength above 800 °C in air is related to fibre surface degradation involving free carbon. Crystallization of SiC and carbon further develops in both fibres subject to either creep or heat treatment at ~1300 °C and above for long periods. The fibres are characterized by steady state creep and greater creep resistance (one order of magnitude) compared to the commercial Nicalon fibre. The experimental fibre has been found to creep above 1280 °C under low applied stresses (0.15 GPa) in air. Significant deformations (up to 14%) have been observed, both in air and argon above 1400 °C. The stress exponents and the apparent activation energies for creep have been found to fall in the range 2–3, both in air and argon, and in the range 200–300 kJ mol^{-1} in argon and 340–420 kJ mol^{-1} in air. The dewrinkling of carbon layer packets into a position more nearly aligned with the tensile axis, their sliding, and the collapse of pores have been proposed as the mechanisms which control the fibre creep behaviour.

1. Introduction

During the last 20 years, important efforts have been made to develop ceramic fibres with high oxidation resistance and good thermomechanical properties, for use as reinforcement in ceramic matrix composites (CMCs) for high-temperature applications. In the mid 70s, Yajima *et al.* [1, 2] developed a process to fabricate small-diameter Si–C–O fibres (i.e. ~ 15 μm) compatible with weaving techniques for the fabrication of CMC parts with complex geometry. This process involves the transformation of a polycarbosilane organic precursor (PCS), according to three main steps: (i) spinning of the melted organic precursor, (ii) curing in air at ~ 180 °C, to render the fibre infusible in order to preserve its cylindrical shape during the final step, (iii) pyrolysis of the cured fibre at a temperature assumed to be of the order of 1200 °C in an inert atmosphere. Many investigators have also explored the possibility of using polymer precursors to prepare not only fibres, but ceramic coatings, thin films, monolithic ceramics, and CMCs as well [3–6]. PCS-derived ceramic fibres have been commercialized for the last decade under the trade name Nicalon. Many of the characteristics of this fibre have made it a potential candidate for reinforcing metals, glass-ceramics and ceramics. However, there have been problems associated with Nicalon fibres which limit their ultimate use as reinforcement of CMCs. Besides SiC (49 mol%), important quantities of free carbon (28 mol%) and an amorphous $SiO_{1.12}C_{0.44}$ phase (23 mol%) [7–9], resulting from the incomplete pyrolysis of the oxygen-cured fibre, are also present in the fibre. At high temperatures (typically above 1200 °C) the silicon oxycarbide phase decomposes, forming SiC and gaseous species such as CO and SiO, whose diffusion through the fibre and reaction with the free carbon are believed to create pores and other defects in the fibre structure [10]. Such a decomposition causes strength and Young's modulus degradations and affects the fibre creep behaviour even in inert atmospheres [9, 11–14].

Because of the inherent thermal instability of Si–C–O fibres and due to increasing processing and end-use temperatures, improved fibres are needed. New routes for the fabrication of ceramic fibres are now being investigated. Okamura [15] reported an alternative approach to prepare SiC fibres, in which curing of PCS could be performed by γ-rays or electron irradiation in vacuum. In this process, the cross-linkage between polymeric chains of the precursor was achieved by directly forming Si–Si bonds between side chains, instead of Si–O–Si bridges as in oxygen

* *Present address*: Institute of Advanced Materials, Joint Research Centre, Petten, The Netherlands.

0022–2461

curing. Compared to the fibres cured in air, the strength of fibres cured by electron irradiation remained almost unaffected after heat treatment to 1400 °C. A slight increase in Young's modulus was even noticed at these temperatures [15, 16].

In this study, the creep behaviour and the microstructural changes of an experimental SiC-based fibre, prepared by electron irradiation of PCS, were investigated in air and argon environments. In addition to the need for a time-dependent property database, the creep study of this fibre was motivated by the need to establish the mechanism(s) of creep and to understand the difference in behaviour with the commercial Si–C–O-based fibre.

TABLE I Fibre properties reported by the manufacturer

	Hi-Nicalon	CGN
Fibre diameter (μm)	14	14
Number of filaments (fil./yarn)	500	500
Tex (g/1000 m)	200	210
Tensile strength (GPa)	2.8	3.0
Tensile modulus (GPa)	270	220
Elongation (%)	1.0	1.4
Density (kg m^{-3})	2740	2550
Specific resistivity (Ω cm)	1.4	10^3–10^4
Chemical composition (wt %) Si	63.7	56.5
C	35.8	31.2
O	0.5	12.3

2. Experimental procedure

2.1 Materials

Two different groups of small-diameter fibres were chosen for detailed creep and rupture studies, the commercial ceramic grade Nicalon fibre (lot 022B, Nippon Carbon Inc., Japan) referred to as CGN fibre, and an experimental fibre, Hi-Nicalon (lots 45 and 62, Nippon Carbon Inc., Japan). The former fibres were chosen because they are the most commonly used small-diameter ceramic fibres available commercially. They were also chosen to serve as a reference fibre to the latter group which were the experimental polycrystalline fibres with a low oxygen content (referred to as Hi-Nicalon) for use as potential reinforcement in CMCs. Two lots of the experimental fibres in the form of tows of approximately 250 filaments each were received at different periods of time. The former version was uncoated; the latter was coated with a polyvinyl alcohol sizing. The commercial CGN fibre was received in spool form coated with a polyvinyl acetate sizing. Prior to the elemental and mechanical analyses, these sizings were removed by dissolution in a mixture of acetone and ethanol at a temperature of ~ 50 °C. The manufacturer-reported data for these fibres are shown in Table I. The oxygen content of the Hi-Nicalon fibre is reported to be only ~ 0.5 wt % whereas it is 12 wt % for CGN.

2.2 Experimental methods

2.2.1. Annealing

Hi-Nicalon fibres were annealed at 1600 °C for 1 and 10 h in argon to enhance phase crystallization and to determine the influence of the grain growth on the creep behaviour of the fibre in argon.

2.2.2. Mechanical testing

The experimental apparatus for high-temperature strength tests in air is the same as used for performing room-temperature tests [17], and consists of (i) a microtensile device with a small capacity load cell (designed and fabricated by SEP, Bordeaux; 0–2 N full scale) and a straining micrometric table (model UT 100 CC, Microcontrol) whose displacements are measured with an accuracy of 0.1 μm through an incremental encoder mounted directly on the d.c. motor of the table, (ii) a small, custom-built electric furnace made of two refractory bricks, each containing platinum heating elements which produce a ~ 30 mm isothermal hot zone, and (iii) a chart recorder of the load–displacement curve. Gripping of the filament was accomplished by inserting the fibre ends into alumina tubes and gluing them with a high-temperature cement consisting of SiO_2, silicon and SiC powders mixed with an alumina-based ceramic adhesive (No. 503, Aremco Products Inc., Ossining, NY), whose composition has been optimized to yield the best clamping of the fibres as well as to delay the apparition of creep at 1400 °C. The test specimen with hot grips was mounted on the tensile system while maintaining the furnace open at a temperature slightly lower than that of the test. High-temperature tests were performed within about 1 min after temperature stabilization.

The single filaments used for creep tests with cold grips were 180 and 270 mm in length, depending on the height of the furnace used in the experiments. As shown in Fig. 1, for tests in argon, each end of the fibre was cemented with the ceramic adhesive to a 20 mm × 5 mm × 1 mm alumina tab as a means of attaching the fibre to the testing system. For creep tests conducted in air, only one end of the fibre was glued on a similar tab. The cement was successively dried for at least 2 h at room temperature and 4 h at 350 °C. Before each test, the average diameter of the fibre was estimated from laser diffraction measurements at several points along the central portion of the test specimen [18]. The fibres were selected for creep test when the variation of their diameters along the hot zone (i.e. 33.5–37.8 mm in argon, and 110 mm in air) was less than ± 0.2 μm. Loads were derived from selected stresses and average diameters.

As shown in Fig. 2, the apparatus for creep testing single filaments in air was designed to test simultaneously three fibres. The fibres were held vertically, with their top tab attached to a solid plate. The bottom ends of the fibres were glued with cyanoacrylate on small diameter steel pins which were fixed to the shaft of inductive transducers (models WC-1, WC-2, WC-5, Hottinger Baldwin Messtechnick Corp., Darmstadt, Germany). In this configuration, the fibre elongation was directly given by the transducer shaft displacement. The three transducers had different

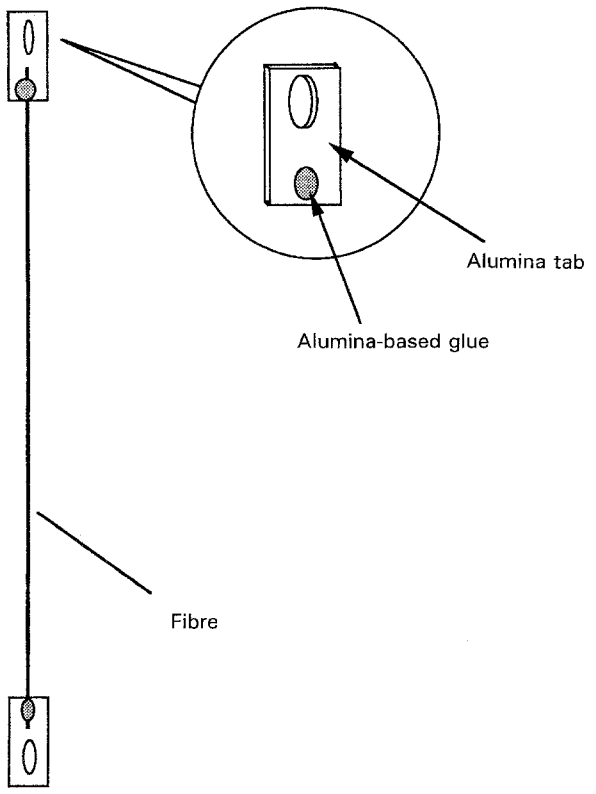

Figure 1 Single-fibre specimen for creep experiments.

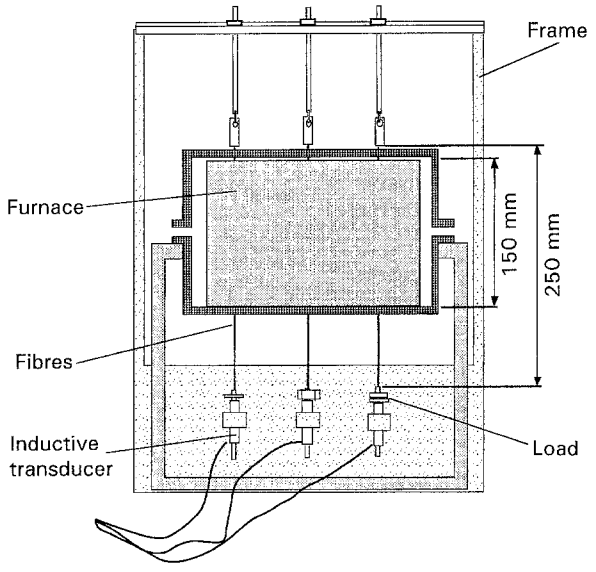

Figure 2 Schematic drawing of the creep apparatus for tests in air.

ranges of linear output (5, 2, and 1 mm/10 V). Because the accuracy of the measure depends on the range of the transducer, and assuming that the fibre creep strain increases with increasing stress, the transducers were selected according to their output range to best fit the desired stresses, i.e. the smaller output range was attributed to the smaller applied stress. The load was applied using calibrated steel rings and screws on the top of the shaft. The minimum available weight of the transducer shaft (i.e. with a 1 mm range) made applied stresses as low as 0.15 GPa possible. The fibres were heated at a rate of 100 °C min^{-1} to the test temperature. The temperature profile along each lateral fibre accounted for a deviation of 20 °C relative to the central fibre. Taking into account these observations, tests were performed at applied stresses from 0.15–0.70 GPa over the temperature range 1180–1300 °C for the CGN fibre, and 1180–1400 °C for the Hi-Nicalon fibre.

Tests were also performed in an argon atmosphere, using a modified test apparatus (custom built furnace, LCTS, Bordeaux) initially constructed for torsion tests [18]. The creep apparatus for tests in argon was a combination of three systems: (1) system for the mechanical testing of specimens with cold grips; (2) system for the temperature control; and (3) system for the environment control. As shown in Fig. 3, the system for testing was designed to fix one end of the test specimen on the top of the furnace to a small-capacity load cell (model Q 11, range 100 g, Hottinger Baldwin Messtechnick Corp., Darmstadt, Germany) to verify the accuracy of the applied load, and to attach the other end to a horizontal lever which was loaded prior to the heat-up schedule using dead weights. In this case, a capacitive transducer (model LVC 1-12, range 12.5 mm, Mesuretron, Butler, PA) mounted on a holder and connected to a signal conditioner (model SCM-03, Electronic Instrument Research, Ltd, Irwin, PA) was chosen to measure the fibre elongation to avoid any perturbations between the transducer signal and the r.f. induction furnace. The vertical shaft of the LVC transducer was connected to the other end of the lever. When the lever rotated, the lower end of the fibre and the LVC shaft moved simultaneously, but in the opposite direction. The temperature control system consisted of a graphite-lined induction furnace, supplied by an r.f. power

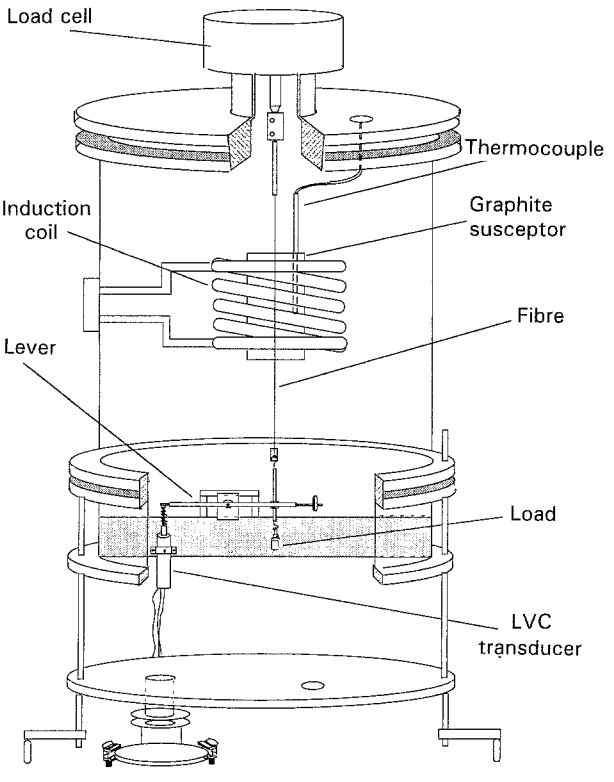

Figure 3 Schematic drawing of the single-filament creep apparatus for argon tests.

generating source (model GHF 3 AP, Celes, Lautenbach, France), and a temperature controller. The fibre was heated at a rate of 70 °C min^{-1} to the test temperature. The environment was controlled using a water-cooled stainless steel chamber which isolated the fibre and test system from the room ambience, a vacuum system with a turbomolecular pump (model PT 50, Leybold, Germany), and a gas supply source. Prior to each test, the chamber was pumped down to 10^{-3} Pa. The creep strain was derived from the transducer displacement which was printed on a chart recorder and recorded by a computer for later analysis. Tests were performed at applied stresses from 0.15–0.70 GPa over the temperature range 1200–1400 °C for CGN fibres and 1200–1600 °C for Hi-Nicalon fibres. Tests were performed on heat treated Hi-Nicalon fibres from 0.30–0.70 GPa at 1300 and 1400 °C.

Under the current design, the creep deformation was obtained by measuring the total elongation of the specimen. Because of the unavoidable temperature distribution along the fibre length, portions of fibre away from the hot zone also contributed to the measured total creep elongation. An effective gauge length, i.e. a length having a unique creep rate under a uniform temperature had to be determined for each test temperature. An accurate calculation of the creep rate requires not only the temperature distribution along the fibre axis, but also the properties of the materials, that is, the relationship between creep rate and temperature. Such analysis to determine the effective gauge length can be found elsewhere [19]. The problem associated with the water-cooled inductor of the apparatus used for argon experiments was that the temperature profile along the fibre length became sharper as the test temperature increased. As a consequence, an effective gauge length had to be determined for each given test temperature. These effective gauge lengths ranged from 30–37 mm. The procedure was much easier in air than in argon. In this case, the temperature distribution was the same for any fibre position in the furnace, except that profiles for lateral fibres were simply shifted to temperatures ~ 20 °C lower than for the central fibre. Values for the effective gauge lengths determined at 1200 and 1400 °C varied little and a unique gauge length of 110 mm was used for tests performed in air.

2.2.3. Elemental and microstructural analyses

The elemental analysis of the as-received fibre was performed on fibre cross-sections by electron-probe microanalysis EPMA (Camebax 75, Cameca, Courbevoie, France), in the wavelength dispersion mode (the curved analysers being PET for SiK_α and multilayered PCI for both CK_α and OK_α). The surface composition of as-received fibres was obtained using Auger electron spectroscopy (AES). AES analyses were performed with a microanalyser (PHI-590 SAM, Perkin-Elmer Corp., Norwalk, CT), with a 1 μm spot size, using the depth profiling mode at an estimated sputtering rate of 1.5 nm min^{-1} (reference Ta_2O_5) on single fibres mounted on indium foil. The intensities of selected Auger electron transitions (i.e. LVV for silicon, KLL for carbon, and KLL for oxygen) were recorded as a function of the thickness of material which has been sputtered. Heat treated and crept fibres were also characterized by means of AES analyses using the same depth profiling technique but at higher sputtering rates.

The structures and morphologies of the crept specimens were characterized by means of scanning (SEM) and transmission (TEM) electron microscopies. Specimen fracture surfaces after creep tests were examined in a scanning microscope (JSM 840 A, Jeol, Tokyo, Japan). TEM analyses using bright-field imaging (BF), dark-field imaging (DF), selected-area diffraction (SAD), and lattice-fringe imaging (LF), were performed using 200 and 300 kV microscopes (Jeol 2000, Jeol, Tokyo, Japan; CM 30, Philips Electronic Instruments Inc., Eindoven, Netherlands). TEM examination used two complementary techniques: longitudinal fibre sections to study the microstructure of the fibre core in the creep direction, and cross-sections to characterize the possible microstructural changes in the radial direction. Fibre segments (~ 5 mm) were coated with a small quantity of an alumina powder suspension in a silicate solution (No. 597, Aremco Products Inc., Ossining, NY). The coating procedure was repeated several times (up to ten), after each layer had been dried at room temperature. The resulting blocks were cut in ~ 1 mm thick slices which afterwards were embedded under vacuum in an epoxy resin. The resin was cured at ~ 90 °C for 24 h, followed by the trepanning and polishing operations. The resulting 60–80 μm thick foils were finally thinned in an ion milling machine (Gatan Inc., Warrendale, PA) until perforation of the fibre. The low-magnification micrograph in Fig. 4 shows the cross-section of

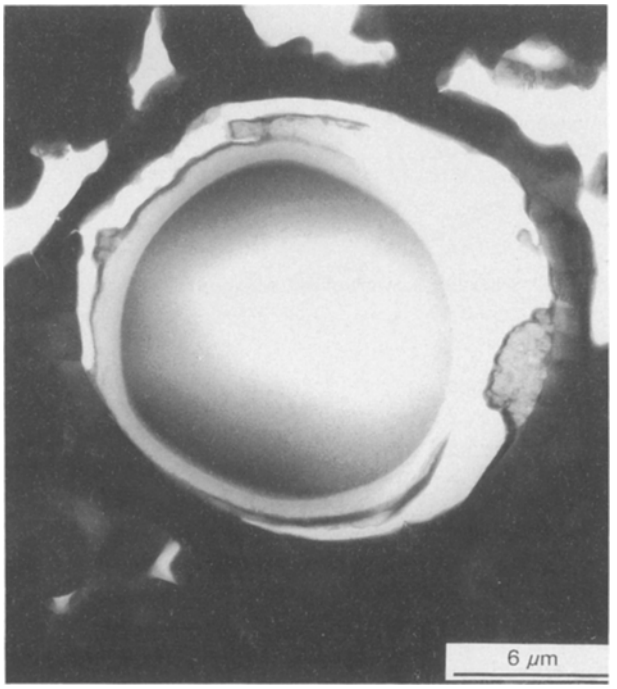

Figure 4 Typical TEM specimen cross-section of a fibre tested at 1500 °C under an applied stress of 0.45 GPa in argon, $t_f = 5.6$ h, $\varepsilon_f = 2.27\%$.

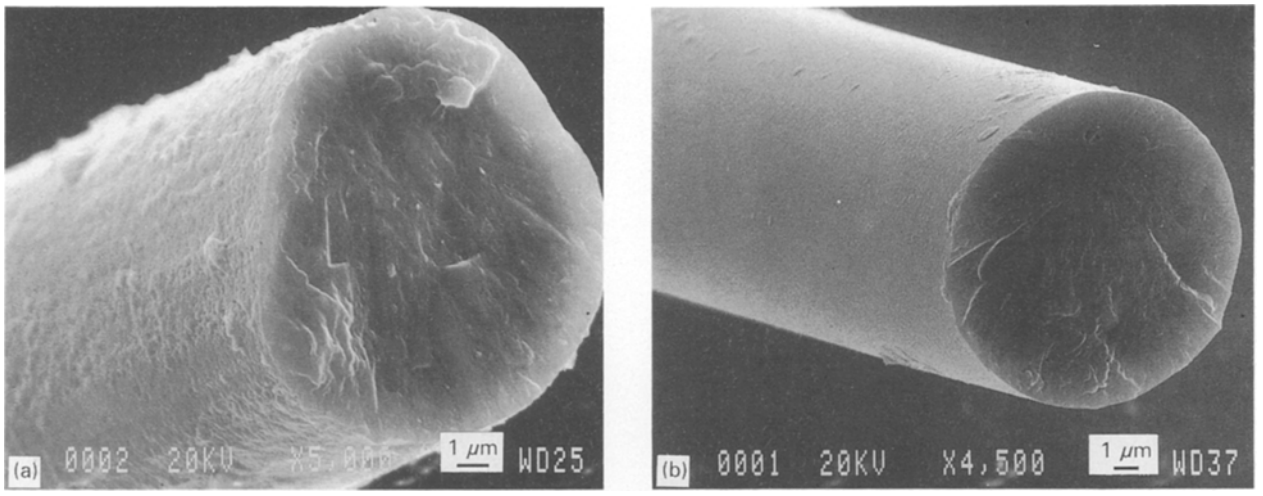

Figure 5 Scanning electron micrographs of (a) Hi-Nicalon and (b) CGN fibres.

a specimen tested in argon. The longitudinal sections were prepared by ion thinning fibres that had been glued between two centre-holed TEM grids.

3. Results

3.1. Properties of as-received fibres

3.1.1. Characteristics of CGN and Hi-Nicalon fibres

A typical Hi-Nicalon fibre, as observed in the SEM, is shown in Fig. 5a. Fibres were usually found to have a rough surface and a non-uniform cross-section longitudinally and circumferentially; this latter feature can be observed on the TEM cross-section in Fig. 4. On the other hand, the CGN fibres had a smooth surface and a round cross-section, as seen in Fig. 5b.

3.1.2. Elemental composition

The average elemental compositions of the fibres, obtained using EPMA, are indicated in Table II. The oxygen weight percentage of the Hi-Nicalon fibre, i.e. 0.5 wt%, is in good agreement with the manufacturer's data. By comparison, the oxygen content in the CGN fibre is 10 wt%. On the other hand, silicon and carbon percentages in the Hi-Nicalon fibre differ slightly from the manufacturer-reported data. From the elemental composition in Table II, it is obvious that the Hi-Nicalon fibre contains an excess of carbon relative to stoichiometric SiC. Neglecting oxygen and considering stoichiometric SiC, one can estimate the molar composition of the Hi-Nicalon fibre. Results account for 35.4 mol% of free carbon and 64.6 mol% of SiC in the fibre. Based on results from elemental and microstructural analyses, the molecular composition of the CGN fibre has previously been determined. It was proposed that the fibre consists of three phases which are SiC, carbon, and an $SiO_{1.12}C_{0.44}$ phase, whose corresponding molar percentages are 49, 28, and 23 [9]. It is thus believed that the Hi-Nicalon fibre contains more free carbon and SiC than the CGN fibre.

The AES depth profile of the Hi-Nicalon fibre, in Fig. 6, indicates a $\sim$ 50 nm thick surface layer whose composition differs from that of the fibre bulk. This layer rich in oxygen is also found to contain silicon and carbon. A very similar oxygen-rich layer has also been observed on the surface of CGN fibres [11].

3.1.3. Phase structure

The phase structure of the as-received Hi-Nicalon fibre was investigated by TEM analysis. Fig. 7a and b show the bright- and dark-field images of the fibre obtained near the central region. As shown on the SAD pattern in the inset of Fig. 7b, three distinct rings corresponding to the 1 1 1, 2 2 0 and 3 1 1 reflections of β-SiC are apparent. In the 1 1 1-centred dark-field image, the reflection of β-SiC can be easily recognized. A value of $\approx$ 5 nm has been obtained for the average β-SiC grain size. However, grains as large as 10 nm

TABLE II Elemental and molar compositions of as-received Hi-Nicalon and CGN fibres

		Elemental composition				Molar composition		
		Si	C	O		SiC	C	SiO_xC_y
Hi-Nicalon	at%	39	60.4	0.6	mol%[a]	64.6	35.4	
	wt%	59.8	39.7	0.5	wt%	85.9	14.1	–
CGN	at%	39.6	48.6	11.8	mol%[b]	49	28	23
	wt%	59	31	10	wt%	56	10	34
						$x = 1.12$, $y = 0.44$[b]		

[a] Determined from the rule-of mixture.
[b] Calculated from elemental and structure compositions. For more details, see [9].

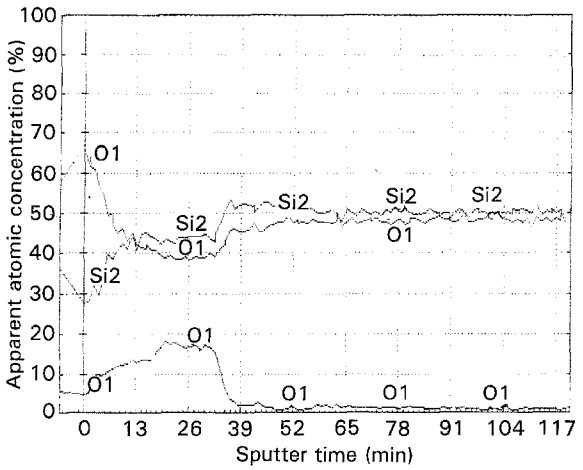

Figure 6 AES semi-quantitative analysis (peak-to-peak mode) of the surface of the Hi-Nicalon fibre. Profile shows an oxygen-rich layer on the fibre surface (sputtering rate 1.5 nm min^{-1}; reference Ta_2O_5).

were easily found from dark-field analysis of the fibre. By comparison, the average size of β-SiC grains is $\approx$ 1.7 nm in the CGN fibre [11]. Important quantities of aromatic carbon structures have been detected in the Hi-Nicalon fibre using high-resolution TEM. Arrows in Fig. 8 show these structures which are found to be very similar to the basic structural units (BSU) of the carbon, and are seen to exist into some wrinkled, continuous layers. These carbon BSUs appear as either a single layer or stacked in small numbers (i.e. up to 5) between SiC grains. Compared to the CGN fibre [9], the Hi-Nicalon fibre was found to contain more and better-organized free carbon.

3.1.4. Strength and Young's modulus

As seen in Fig. 9a and b, the Hi-Nicalon fibre has higher strength and Young's modulus at room-temperature than the CGN fibre, the increase being $\sim$ 40% in both cases. For both fibres, the decrease in strength and Young's modulus becomes significant when the temperature is above 800 °C, where creep of CGN fibres is about to become measurable (i.e. $\sim$ 910 °C) [20]. At 800 °C, the fibres experienced a loss in strength of $\sim$ 17%. At 1300 °C, the strengths of both fibres were only 56% of those measured at room temperature, and the Young's moduli were about 68% and 78% of those of the as-received CGN and Hi-Nicalon fibres, respectively. These results are in good agreement with previously reported data for CGN and Hi-Nicalon fibres tested in air [21, 22]. However, these results are considerably different from those obtained for various polycrystalline SiC materials, for which the degradation of strength and modulus is just about to begin at 1300 °C [23]. As shown in Fig. 10a and b, the experimental fibre contains large processing defects. These defects are responsible for the wide strength distribution observed at low temperatures. Fig. 11 shows the fracture surface of a fibre tested at 1300 °C in air (1.094 GPa), which had a much lower strength than the average (1.864 GPa). Blisters, resulting from surface oxidation, were in part responsible for the low fibre strength at

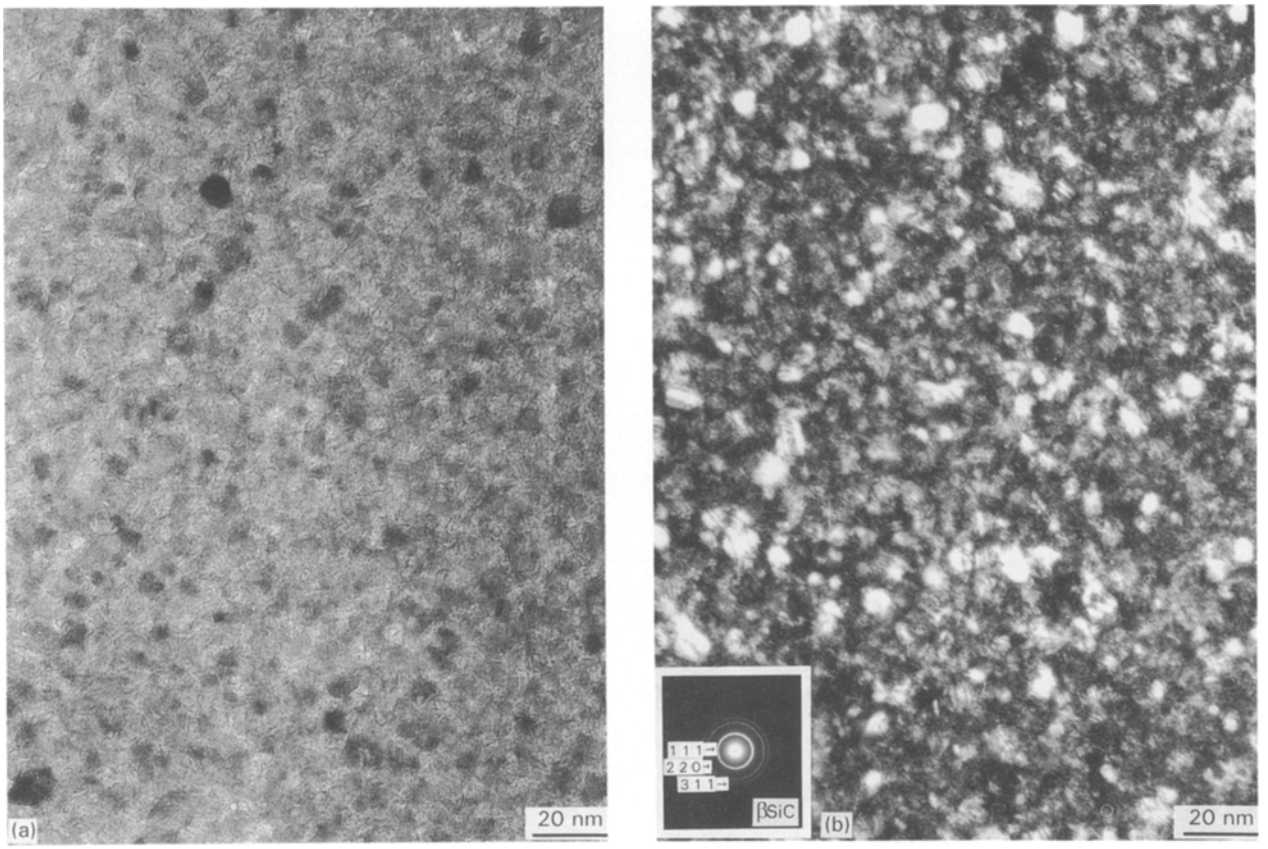

Figure 7 (a) Bright-field transmission electron micrograph of the core of the Hi-Nicalon fibre. (b) 1 1 1 SiC dark-field micrograph and SAD pattern (inset) of the core of the Hi-Nicalon fibre. The dark field indicates a mean crystallite size of 5 nm.

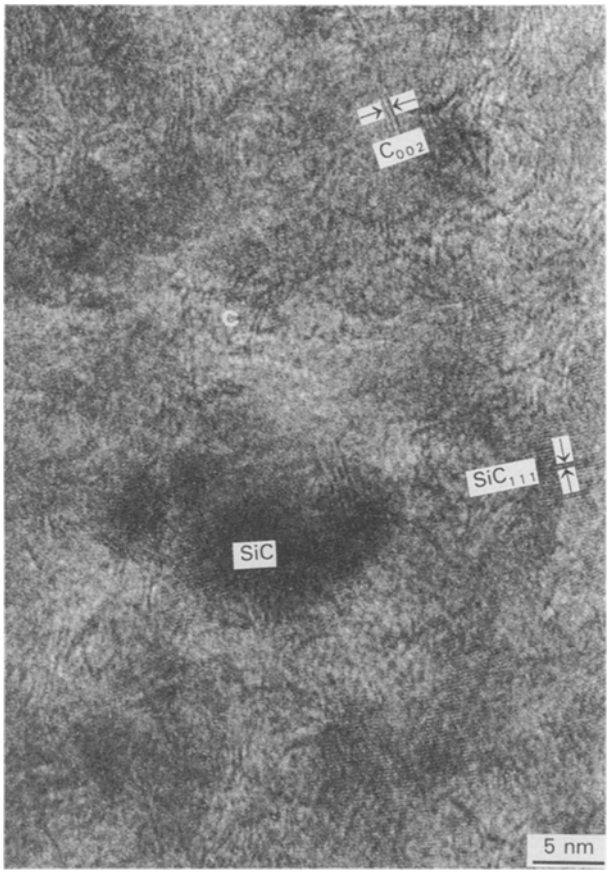

Figure 8 Lattice fringe imaging of the as-received Hi-Nicalon fibre. Arrows show the 0 0 2 carbon and the 1 1 1 SiC planes.

high temperatures. Although these flaws may have caused premature fibre failure, the features of the fibre fracture surfaces resembled closely those of glass, which contain typical mirror, mist, and hackle regions.

3.2. Structure of annealed fibres

The effects of annealing in argon at 1600 °C on the crystallization of the Hi-Nicalon fibre, as revealed by TEM, are shown in Fig. 12a and b. The bright-field image of a longitudinal TEM thin foil shows that large grains have developed during a 1 h anneal. The corresponding SAD pattern with distinct spotty rings of SiC is shown in the inset of Fig. 12a. An average SiC grain size of $\sim$ 20 nm was obtained from the dark-field image in Fig. 12b. On the other hand, the CGN fibre had entirely decomposed at this temperature, with β-SiC grain sizes reaching several micrometres. Compared to the as-received fibres, the heat-treated Hi-Nicalon fibres were found to contain better-organized carbon BSUs. The lattice fringe image in Fig. 13a shows a distorted stacking of several continuous carbon layers whose length and thickness, characterized by the parameters L_2 and L_c, respectively, are approximately 47 and 4 nm. A more pronounced increase in crystallinity occurred after 10 h annealing at 1600 °C. In Fig. 13b, the stackings of carbon layers form a continuous network throughout the image (with an estimated L_2 parameter being equal to 75 nm). The number of stacked carbon layers can be important (i.e. more than 20), corresponding to $L_c = \sim 7$ nm.

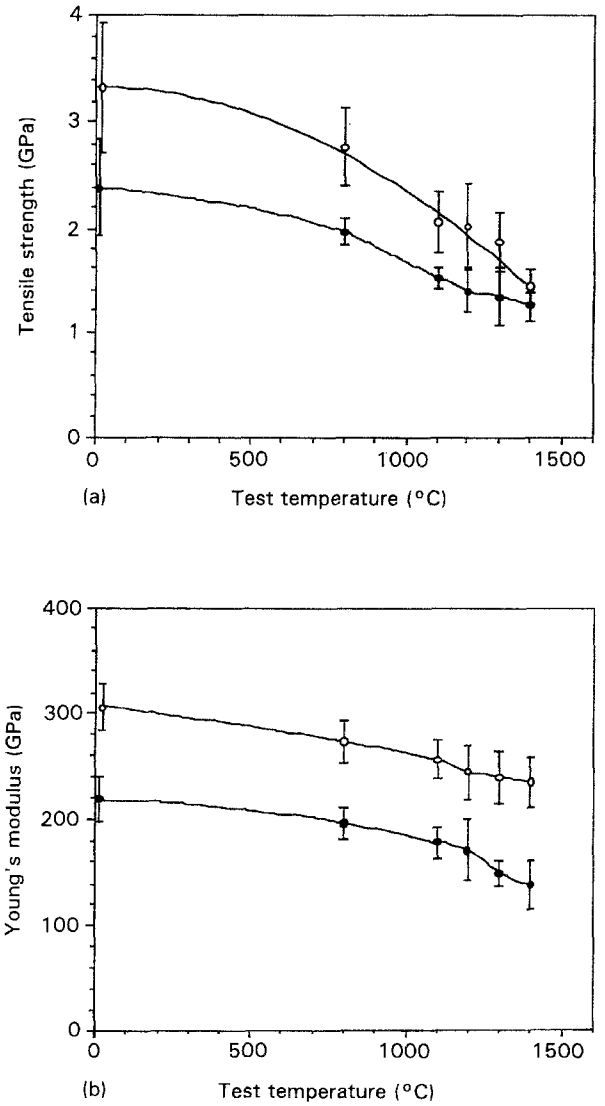

Figure 9 High-temperature short-term strength tests of (○) Hi-Nicalon and (●) CGN fibres. (a) Tensile strength, (b) Young's modulus. The error bars represent the standard deviation.

3.3. Results of creep experiments

Results from creep tests on single CGN fibres in argon were presented and discussed previously and will not be included in this paper [9, 14, 20]. Only results from tests performed in air will be presented to emphasize the microstructural changes and the difference in creep behaviour with the Hi-Nicalon fibre.

3.3.1. Creep curves

Typical creep strain versus time curves for CGN (NL 202) and Hi-Nicalon fibres tested in air are represented in Fig. 14a–c, for different temperatures and applied stresses, σ_{app}. The Hi-Nicalon fibre was found to be more creep-resistant than the CGN fibre, i.e. its creep strain was lower than that of the CGN fibre during its entire lifetime. The creep of the Hi-Nicalon fibre was characterized by a long steady-state domain. On the other hand, the curves indicate that, in most cases, the CGN fibres exhibited only primary creep, that is, the creep rate decreased continuously with time during the entire experiment.

A more detailed representation of the creep curves of Hi-Nicalon obtained in air is indicated in

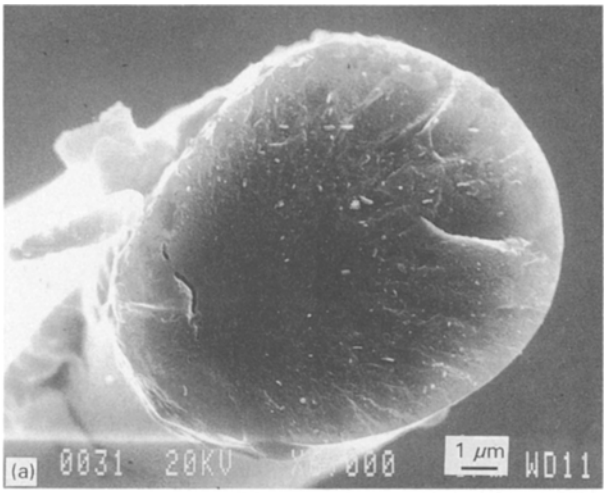

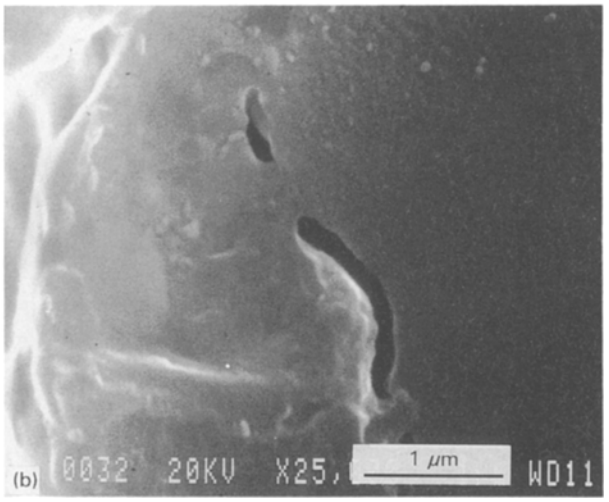

Figure 10 Scanning electron micrographs of a Hi-Nicalon fibre tested at 1200 °C (σ_f% = 1.804 GPa). (a) Fracture surface, (b) magnified view showing internal defect.

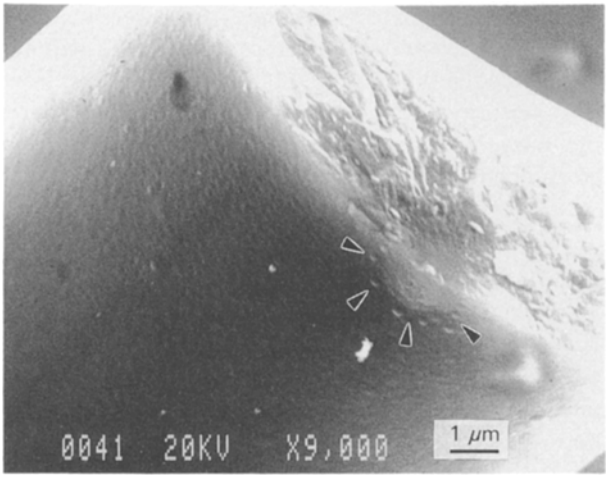

Figure 11 Fracture surface of a Hi-Nicalon fibre showing surface reaction (arrows) resulting from the high-temperature exposure in air (σ_f = 1.094 GPa).

Fig. 15a–d. As previously mentioned, the curves exhibit in addition to the primary creep region, a long steady-state domain. For σ_{app} = 0.15 GPa, creep became measurable above 1280 °C. Under low applied

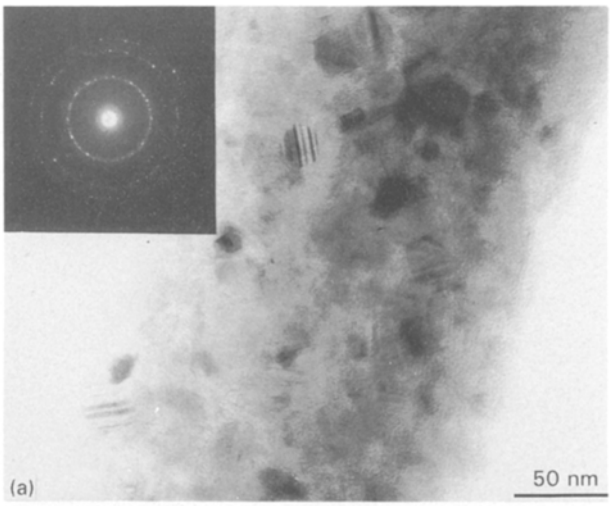

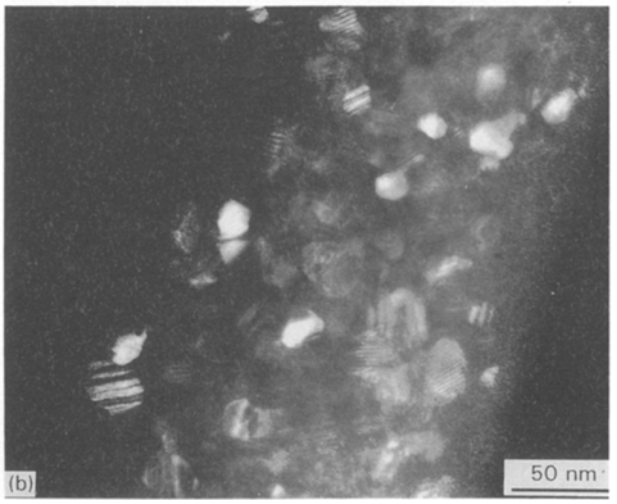

Figure 12 TEM analysis of annealed Hi-Nicalon fibres. (a) Bright field and SAD pattern, and (b) 1 1 1 SiC dark field indicating a mean grain size of 20 nm.

stresses (i.e. 0.15 and 0.19 GPa), values of the strains-to-failure were generally below 1%. Under the most severe testing conditions, high creep strain values were obtained. In all cases, no tertiary creep was observed from experiments conducted in air.

Characteristic creep curves obtained in argon are shown in Fig. 16a and b for as-received fibres tested at different temperatures and applied stresses, and in Fig. 17 for preheat-treated fibres at 1600 °C and tested at 1300 and 1400 °C, respectively. A comparison between Figs 16 and 17 indicates that the primary creep duration was an order of magnitude shorter for the heat-treated fibres than for the as-received fibres (i.e. ~ 50 min versus ~ 500 min). Moreover, the preheat-treated fibres in argon experienced shorter lifetimes. However, in the case of as-received fibres tested in argon, the times-to-failure presented significant scatter to such an extent that only 12% of the tested fibres reached steady state creep. For example, at 1400 °C and 0.45 GPa, 91% of the tested fibres failed within 5 h, whereas the remaining ones lasted for more than 57 h. The creep curves shown in Fig. 16 are, in fact, representative of the most successful tests obtained in argon. Fig. 18 shows the average times-to-failure versus temperature plotted on a semi-log scale. The single-sided error bars which represent one standard

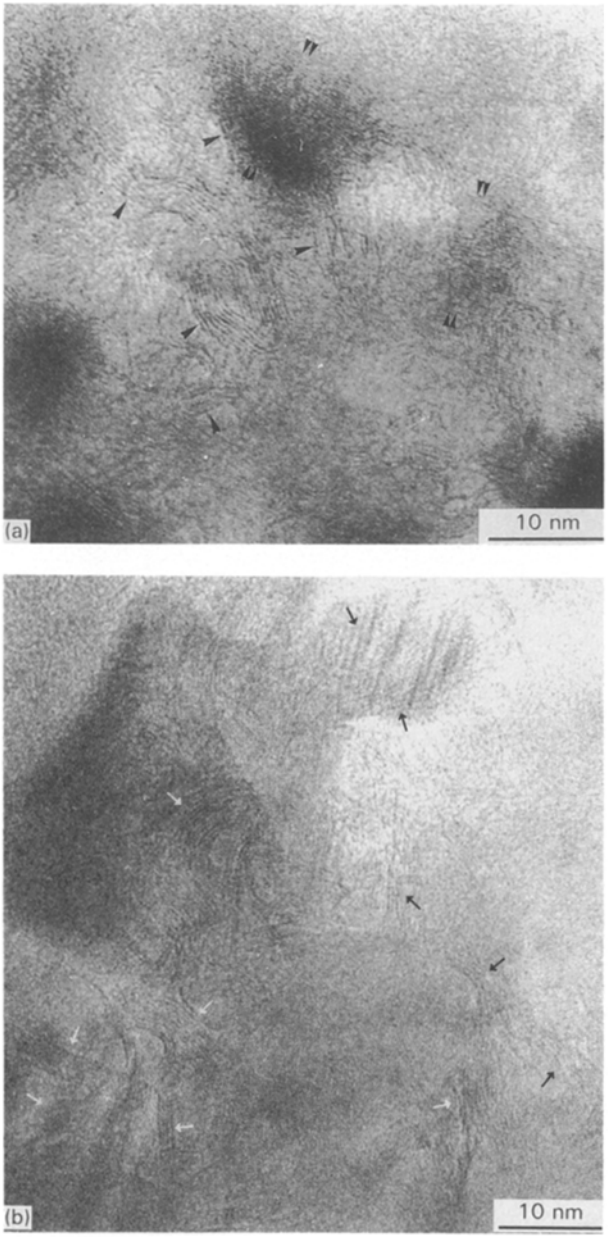

Figure 13 (a) Lattice fringe imaging of a Hi-Nicalon fibre annealed at 1600 °C for 1 h. Single arrow heads show the 0 0 2 carbon layers and double arrow heads show the 1 1 1 SiC planes. (b) Lattice fringe imaging of a Hi-Nicalon fibre annealed at 1600 °C for 10 h. Arrows show the carbon layers.

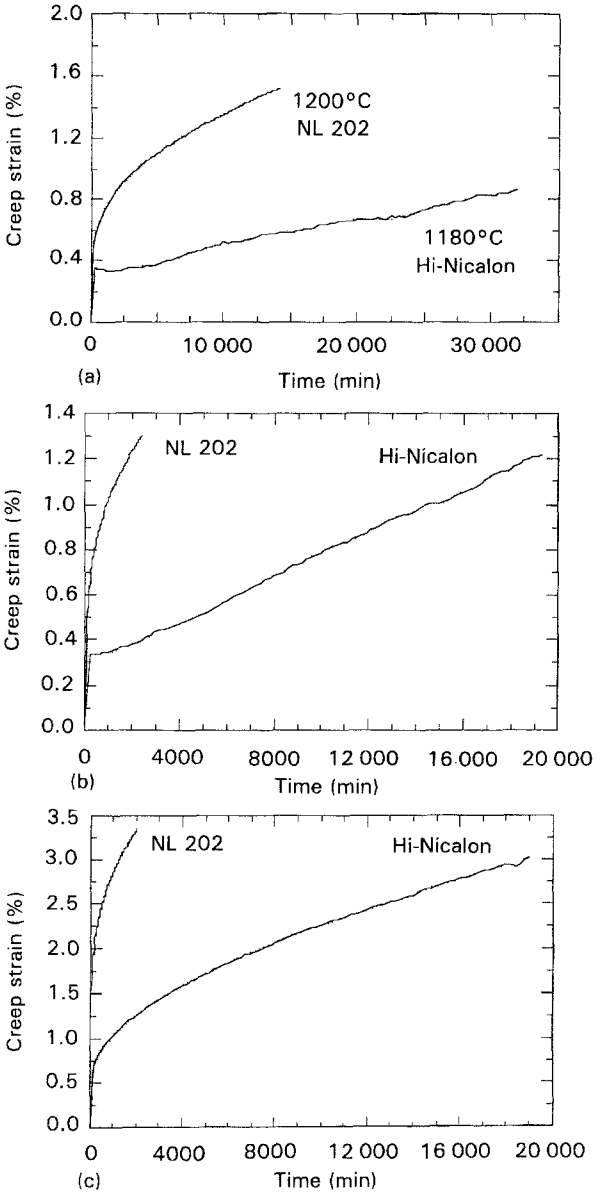

Figure 14 Creep curves for CGN and Hi-Nicalon fibres tested in air at (a) 1180–1200 °C and 0.45 GPa, (b) 1180 °C and 0.70 GPa, and (c) 1300 °C and 0.45 GPa.

deviation, indicate that the data varied drastically. Except for an applied stress of 0.15 GPa, Fig. 18 indicates that generally the times-to-failure followed an exponential decay with increasing temperature. Fibres tested at 1600 °C and 0.70 GPa failed after only 0.1 h but started to creep well before the test temperature was reached. An accelerating creep rate was indeed observed from ~ 1500 °C. The linear regression fit to the data in Fig. 18 furthermore shows that the times-to-failure were less sensitive to an increase of the temperature when the applied stress was increased. The tertiary creep was never observed from the experiments in argon.

3.3.2. Creep parameters

Material parameters obtained from the experiments include the minimum strain rate, $\dot{\varepsilon}_{min}$, defined as the strain rate near failure for primary creep of CGN fibres in air, the steady state creep rate, $\dot{\varepsilon}_{ss}$, given by the linear portion of the creep curves for Hi-Nicalon fibres, the time to failure, t_f, and the strain to failure, ε_f. Results are shown in Table III for fibres tested in air and for fibres tested in argon, respectively. The material parameters, $\dot{\varepsilon}_{min}$, and $\dot{\varepsilon}_{ss}$, are functions of both temperature and applied stress. Results show that $\dot{\varepsilon}_{min}$ and $\dot{\varepsilon}_{ss}$ generally increase with increasing σ_{app} for the same temperature, and with increasing temperature under given applied stresses. Although an important scatter exists in the data, t_f generally decreases with increasing temperatures and applied stresses. As shown in Table III, the Hi-Nicalon fibre exhibited lower creep strains and rates and much longer times-to-failure than the CGN fibre in air. For example, one fibre was tested for more than 530 h without breaking under a stress of 0.45 GPa at 1180 °C. The lifetime of the CGN fibre was only ~ 39 h under the same testing conditions. At high temperatures and applied

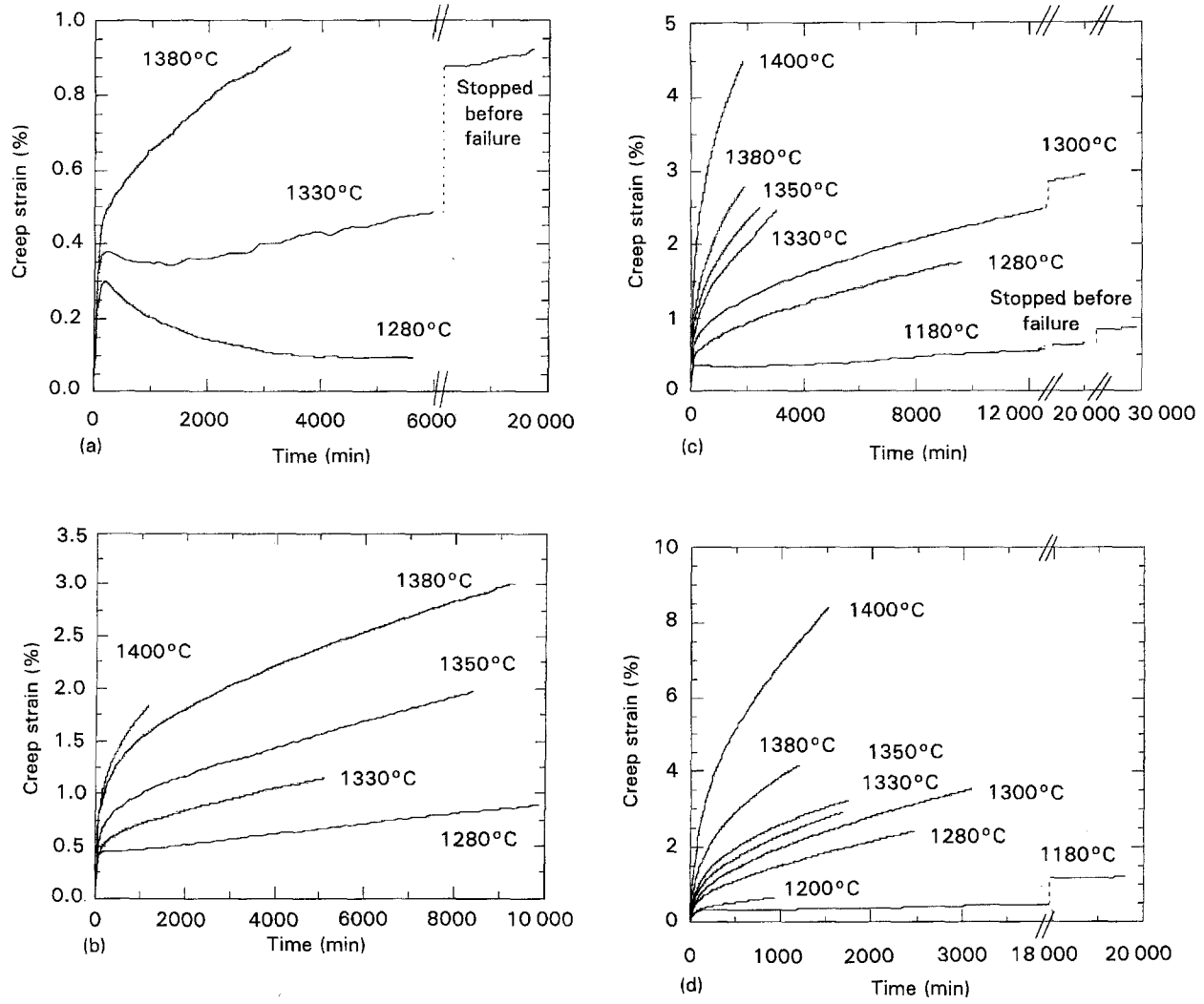

Figure 15 Creep curves for the Hi-Nicalon fibres tested in air for an applied stress of (a) 0.15 GPa, (b) 0.30 GPa, (c) 0.45 GPa and (d) 0.70 GPa.

stresses in air and argon, the Hi-Nicalon fibre experienced significant deformations (i.e. 8.41% at 1400 °C in air, and 14.09% at 1500 °C in argon under a stress of 0.7 GPa).

3.3.3. Effects of temperature and applied stress

The steady state creep behaviour of the Hi-Nicalon fibre was related to the test temperature and the applied stress by the Dorn relation that describes a rate-controlling process [24]:

$$\dot{\varepsilon}_{ss} = A\,\sigma_{app}^{n}\exp(-Q/RT) \qquad (1)$$

where A is a material parameter, n is the stress exponent, Q is the apparent activation energy, R is the perfect gas constant, and T is the absolute temperature. Fig. 19a summarizes data obtained for $\dot{\varepsilon}_{ss}$, plotted against $1/T$ on a semi-log scale. The trend with which $\ln \dot{\varepsilon}_{ss}$ correlates to $1/T$ suggests that Equation 1 describes reasonably well the temperature dependency of the steady state creep rate in air. The apparent activation energies, Q, which were determined from the slope of the linear regressions ranged from 345–423 kJ mol^{-1} over the range of stresses investigated. Fig. 19b plots steady state creep rates against the applied stress, at given temperatures. Stress exponents, n, determined from linear regression analysis, were found to be in the range 1.96–3.04 over the range of temperature investigated. The discrepancy in the values of n may to a certain extent reflect the different aspects of the creep process, because these stress exponents were calculated from creep tests performed at increasing temperatures in air during which the oxidation of the fibre may certainly influence the fibre creep behaviour.

The apparent activation energies for creep of as-received and preheat-treated Hi-Nicalon fibres in argon, determined from the plot of $\dot{\varepsilon}_{ss}$ versus 1/temperature in Fig. 20a, were found to be 193 kJ mol^{-1} for a stress of 0.7 GPa and 292 kJ mol^{-1} for a stress of 0.45 GPa. These energies are lower than those derived from experiments conducted in air. The stress exponents n are indicated in Fig. 20b for the 1300 and 1400 °C data. Values for both fibre types were approximately 2 at 1400 °C, and 3 at 1300 °C for the heat-treated fibre. The lack of data for the as-received Hi-Nicalon fibre over a sufficient range of σ_{app} at 1300 °C prevents determination of n at this condition. As shown in Fig. 20b, values of the creep rates for the preheat-treated fibres tested at 1400 °C were higher than those for the as-received Hi-Nicalon fibre.

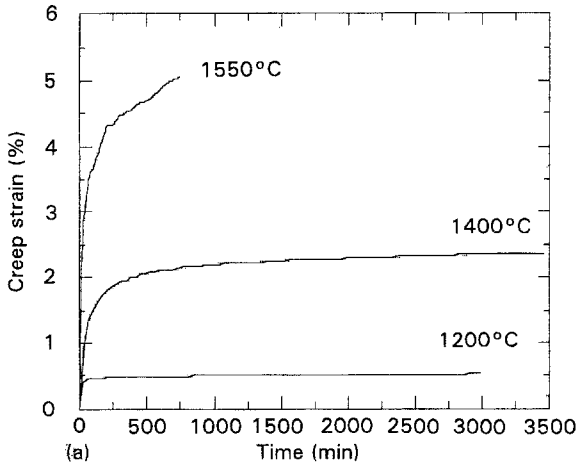

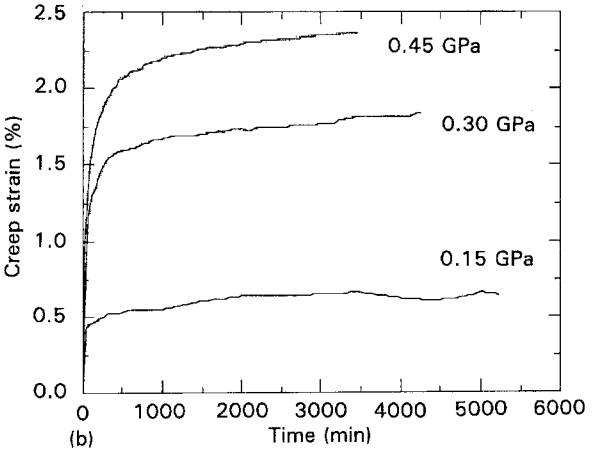

Figure 16 Creep curves for the Hi-Nicalon fibres tested in argon (a) for an applied stress of 0.45 GPa, (b) at 1400 °C.

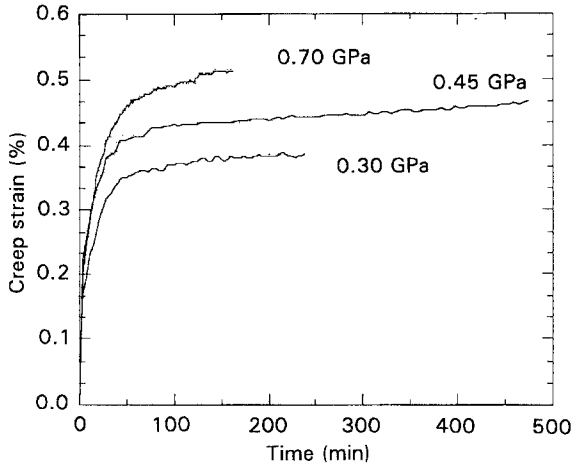

Figure 17 Creep curves for the Hi-Nicalon fibres preheat treated at 1600 °C for 1 h and tested at 1300 °C in argon.

3.3.4. Microstructural analyses

The microstructural analyses using SEM indicated that fibres were subject to severe surface oxidation when tested in air at elevated temperatures. As shown in Fig. 21a, a typical fractured surface consists of two distinct regions: an oxidized porous shell and a remaining non-oxidized core with a rather smooth surface. In the most severe cases, that is, for the longest

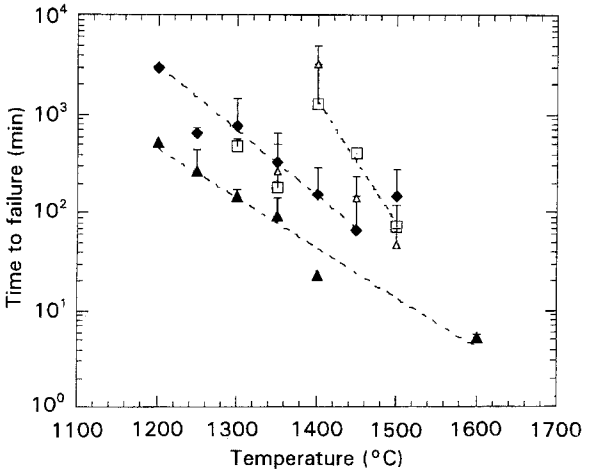

Figure 18 Effect of temperature on the times to failure of as-received Hi-Nicalon fibres on a logarithmic scale. The single-sided error bars represent one standard deviation. Applied stress: (△) 0.15 GPa, (□) 0.30 GPa, (◆) 0.45 GPa, (▲) 0.70 GPa.

exposure times, the oxidation layer can be as thick as one-sixth or one-fifth of the initial fibre diameter (Fig. 21a). However, the thicknesses of the oxidation layers of fibres observed by SEM or AES usually were less than 1 μm (e.g. 0.96 μm at 1380 °C after 155 h). On the other hand, thicker oxidation layers were found on CGN fibres. The CGN fibres also showed exaggerated grain growth, as shown in Fig. 21b. Such a pronounced grain growth was not observed for the Hi-Nicalon fibres in the temperature range selected for the creep tests. The oxidized layer was seen to contain not only pores caused by gas diffusion, but also flaws on its surface. This porous, flawed layer was observed to cause circumferential cracks around the periphery of the fibres. An examination of the fracture modes revealed that the failure of the fibres which were subjected to creep for the longest times (i.e. at low temperatures or under low stresses) were mainly due to the pores formed during the experiment. The change in cross-sectional area due to the growth of the oxide layer, and the stress concentration around a pore were thought to cause the failure of the fibre at a stress much lower than its room-temperature strength. In the case of the CGN fibre, the reduction in strength resulted more from the fibre decomposition, which produced SiC and internal porosity. Fig. 22a and b indicate the change in the fracture mode when the Hi-Nicalon fibre was tested at high temperature and stresses. Fig. 22a shows the ruptured end of a fibre tested for 62.3 h at 1300 °C and 0.45 GPa. Although the fibre had a small strain-to-failure (i.e. $\varepsilon_f = 1.8\%$), important necking was observed at several points along its axis. Necking was also observed at 1280 °C and 0.45 GPa. It was initially thought that this deformation process was caused by the complete transformation of the fibre in silica. However, AES analyses indicated that the thickness of the oxide scales remained limited (i.e. in the particular case of the fibre shown in Fig. 21a, the layer thickness was 0.45 μm). Moreover, a simple calculation revealed that the rupture strength of the elongated portion of the fibre shown in Fig. 22a was very high after such a long time

TABLE III Creep parameters for the Hi-Nicalon and the CGN fibres tested in air and argon.

Atmosphere	T (°C)	σ_a(GPa)	$\dot{\varepsilon}_{ss}(s^{-1})$ Hi-Nicalon	$\dot{\varepsilon}_{min}(s^{-1})$ CGN	t_f (min)		ε_f (%)	
					Hi-Nicalon	CGN	Hi-Nicalon	CGN
Air	1180	0.45	3.10×10^{-9}	4.31×10^{-8}	31821[a]	593	0.86	0.80
		0.70	8.25×10^{-9}	1.82×10^{-8}	19298	2351	1.21	1.3
	1200	0.16		1.40×10^{-9}		15312		− 0.14
		0.45		6.77×10^{-9}		14181		1.52
		0.70	1.47×10^{-8}	8.33×10^{-8}	916	1461	0.65	1.27
	1280	0.15	0	-4.81×10^{-8}	5626	773	0.09	0.02
		0.30	5.39×10^{-9}		9833		0.89	
		0.45	1.73×10^{-8}	2.65×10^{-7}	9612	204	1.76	0.84
		0.70	7.08×10^{-8}		2477		2.44	
	1300	0.45	2.09×10^{-8}	8.23×10^{-8}	19010	2052	3.02	3.36
		0.70	1.02×10^{-7}		3100		3.54	
	1330	0.15	5.21×10^{-9}		19731[a]		0.92	
		0.19	8.22×10^{-9}		6768		0.71	
		0.30	1.60×10^{-8}		5101		1.15	
		0.45	6.39×10^{-8}		3032		2.72	
		0.70	1.33×10^{-7}		1678		2.92	
	1350	0.19	1.00×10^{-8}		5690		0.78	
		0.30	2.07×10^{-8}		8403		1.98	
		0.45	7.29×10^{-8}		2448		2.51	
		0.70	1.42×10^{-7}		1728		3.23	
	1380	0.15	1.54×10^{-8}		3446		0.93	
		0.30	3.54×10^{-8}		9289		3.01	
		0.45	1.02×10^{-7}		1881		2.79	
		0.70	2.56×10^{-7}		1193		4.18	
	1400	0.30	9.15×10^{-8}		2616		1.96	
		0.45	2.21×10^{-7}		1851		4.49	
		0.70	4.60×10^{-7}		1520		8.41	
Argon	1200	0.45	2.11×10^{-9}		2992		0.59	
		0.70	2.76×10^{-8}		535		0.53	
	1250	0.45	6.56×10^{-9}		722		0.51	
		0.70	5.44×10^{-8}		441		0.61	
	1300	0.30	4.45×10^{-9}[b]		238[b]		0.38[b]	
		0.45	1.41×10^{-8}[b]		473[b]		0.47[b]	
		0.70	6.31×10^{-8}[b]		160[b]		0.44[b]	
	1400	0.15	1.11×10^{-9}		5042		0.65	
		0.30	5.01×10^{-9}		4258		1.87	
		0.45	2.73×10^{-8}[b]		286[b]		0.57[b]	
			1.13×10^{-8}		3451		2.38	
			4.98×10^{-8}[b]		359[b]		0.59[b]	
	1500	0.70	4.18×10^{-7}		1288		14.09	
	1550	0.45	2.14×10^{-7}		748		5.05	

[a] The fibre did not fail at the end of the test.
[b] Hi-Nicalon fibres preheat treated in argon.

(i.e. ~ 1.7 GPa). Fibre necking tended to be more uniform along the fibre axis at higher temperatures, as shown in Fig. 22b for a fibre which deformed 4.49%. The SEM analysis of Hi-Nicalon fibres tested in argon did not reveal any changes in the morphology of the fracture surfaces because the investigated fibres generally had short lifetimes. For the few fibres which had longer times-to-failure, the observed fibre ends which had been collected did not reveal any fibre necking, nor did they show any microstructural degradation (i.e. grain growth, porosity) as did the CGN fibres. Instead, they had smooth fracture surfaces. The AES analysis conducted on the fibres which showed premature failure in argon, indicated the presence of a thin carbon rim on the fibre surface. This carbon layer was thought to be caused by the active oxidation of SiC from the residual oxygen present in the test atmosphere and/or originating from the oxygen-rich surface of the as-received fibres.

Evidence was found using TEM that crystallization in the Hi-Nicalon fibres occurs both in air and argon. Table IV summarizes the average SiC grain sizes of several fibres subjected to creep under different testing conditions, as determined from the 1 1 1 SiC dark-field analyses. Table IV indicates that the rate of crystallization clearly increased with temperature. After 14.6 h at 1300 °C in argon, there was no change of the SiC crystallinity. Crystallization occurred at 1400 °C after 57.5 h in argon and 25.3 h in air. The corresponding average SiC grain sizes had increased from ~ 5 nm to 15–20 nm. Crystallization further developed at 1500 °C after 21.5 h and at 1600 °C after only 0.1 h, as shown in Fig. 23, where grains as large as 50 nm are observed. Results from AES analyses of fibres exposed

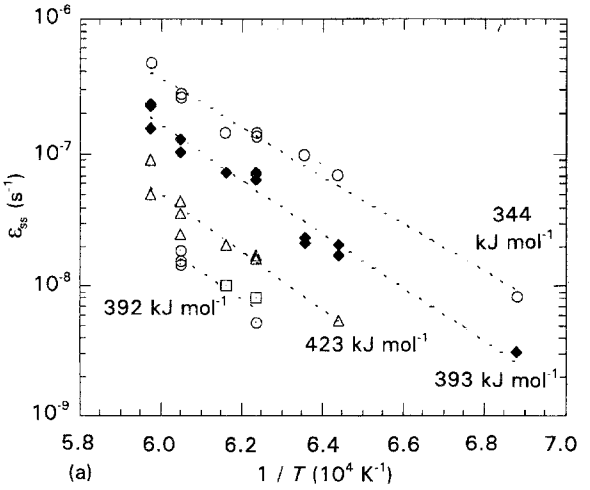

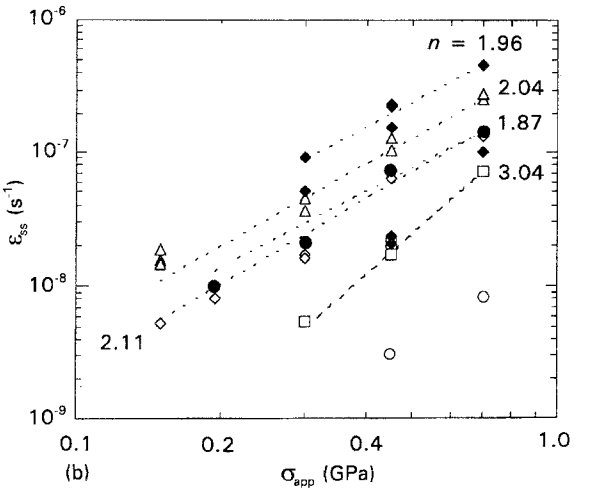

Figure 19 Dorn plots for Hi-Nicalon fibres tested in air. (a) Steady state creep rate versus reciprocal temperature at (○) 0.15 GPa, (□) 0.194 GPa, (△) 0.30 GPa, (◆) 0.45 GPa, (○) 0.7 GPa. (b) Steady state creep rate versus applied stress at (○) 1180 °C, (□) 1280 °C, (◆) 1300 °C, (◇) 1330 °C, (●) 1350 °C, (△) 1380 °C, (◆) 1400 °C.

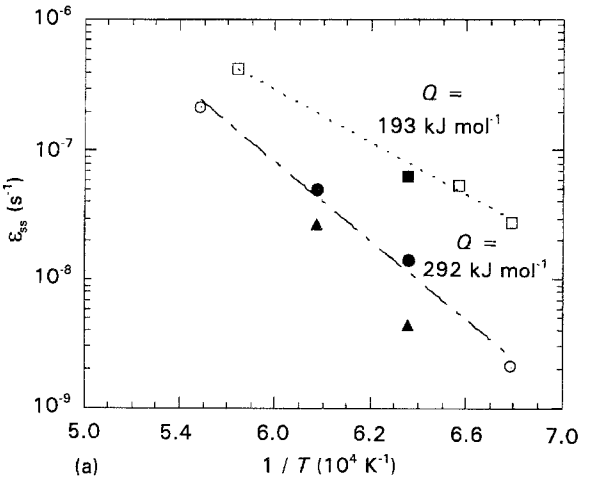

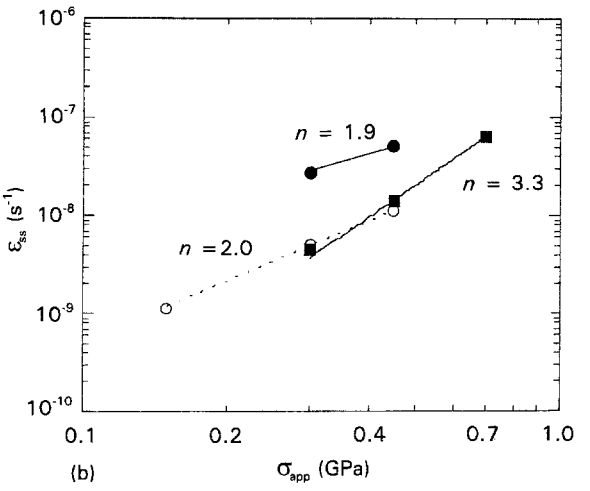

Figure 20 Dorn plots for Hi-Nicalon fibres tested in argon. (a) Steady state creep rate versus reciprocal temperature at (○) 0.45 GPa and (□) 0.7 GPa for as-received fibres, and at (▲) 0.3 GPa, (●) 0.45 GPa and (■) 0.7 GPa for preheat-treated fibres. (b) Steady state creep rate versus applied stress at (○) 1400 °C for as-received fibres, and at (■) 1300 °C and (●) 1400 °C for fibres preheat-treated in argon for 1 h at 1600 °C.

to oxidation during creep indicated that the oxygen penetration remained very limited inside the fibre beneath the oxide scale. TEM analyses on fibre cross-sections confirmed that there was no degradation of the fibre bulk, as it can be seen in Fig. 24. Furthermore, no gradient in grain growth in the radial direction was observed. TEM confirmed the SEM observations that the oxide scale was not well bonded to the fibre surface. Besides SiC grains, of major interest was the state of crystallization of the carbon. Two samples that were tested in air and argon at 1400 and 1500 °C under a stress of 0.7 GPa and that deformed 8.41% and 14.09%, respectively, were examined using TEM. The BSUs or stacks of aromatic layers were found to be more ordered than in the as-received fibre. As shown in Fig. 25 for the material subjected to creep in air, stacks of aromatic carbon layers that are 2–8 nm thick and up to 50 nm long were found preferentially oriented in the creep direction. The SAD pattern in the inset of Fig. 25 shows weak arcs corresponding to the 0 0 2 lattice reflection of carbon, indicating that a low degree of anisotropy is associated with strains of over 8%. The two faint arcs of the 0 0 2 reflection were not observed on the SAD patterns of as-received fibres and fibres that underwent limited creep deformations.

4. Discussion

4.1. General considerations

Although the Hi-Nicalon fibres showed significantly higher tensile strength and Young's modulus than the CGN fibres at temperatures below 1200 °C in air, no significant difference in the retention of strength and Young's modulus was observed between both fibres. Among the various factors influencing the mechanical properties of SiC-based fibres, the following has been already identified: (1) quantity of oxygen, (2) size of β-SiC crystals and state of crystallization, (3) quantity of free carbon [25]. In the present study, both investigated fibres were found to contain free carbon. Earlier microstructural analyses indicated that fibres are subject to severe surface oxidation when tested in air at elevated temperatures. Possible equations corresponding to chemical reactions that may occur at

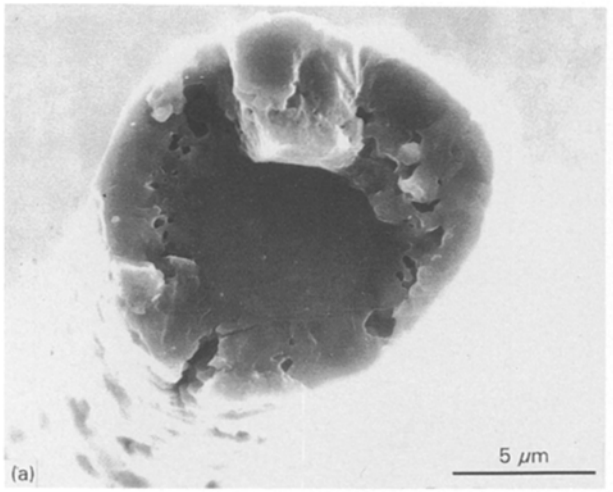

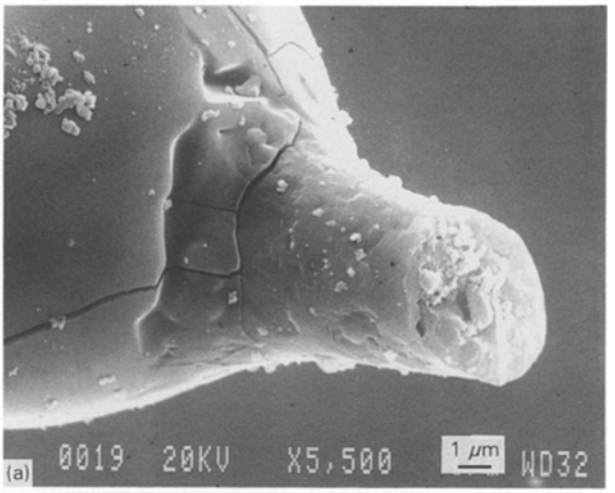

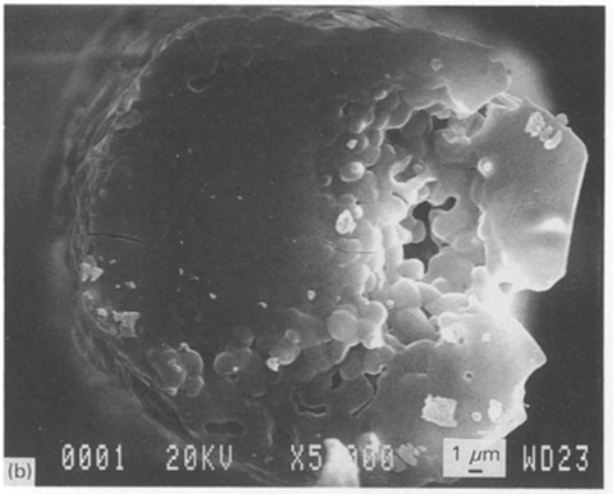

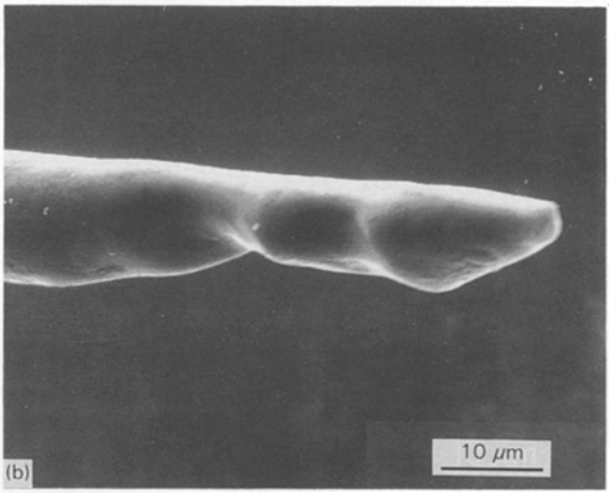

Figure 21 Fracture surfaces after creep exposure in air of (a) a Hi-Nicalon fibre tested for 531 h at 1180 °C and 0.45 GPa ($\varepsilon_f = 0.86\%$), showing the smooth fracture surface and the thick, defective oxidation layer, (b) a CGN fibre tested for 255 h at 1200 °C and 0.15 GPa ($\varepsilon_f = -0.45\%$), showing grain growth.

Figure 22 Ruptured ends of Hi-Nicalon fibre after creep exposure in air, showing necking at (a) 1300 °C and 0.45 GPa (62.3 h, $\varepsilon_f = 1.77\%$), and (b) 1400 °C and 0.45 GPa (30.9 h, $\varepsilon_f = 4.49\%$).

high temperatures include

$$SiC + 3/2\ O_2 \rightarrow SiO_2 + CO \quad (2)$$

$$C + 1/2\ O_2 \rightarrow CO \quad (3)$$

$$SiO_2 + 3C \rightarrow SiC + 2CO \quad (4)$$

The decrease in fibre strength at low temperatures (i.e. 800 °C) is mostly controlled by Reaction 3. The formation of a thin SiO_2 scale at higher temperatures, according to Reaction 2, is also accompanied by CO gas evolution (Reactions 2–4). The CGN fibre additionally has an amorphous $SiO_xC_{1-(x/2)}$ phase which decomposes above 1200 °C according to the following overall equation [9]:

$$4SiO_xC_{1-(x/2)} = (4 - 3x)\,SiC + x\,CO + 3x\,SiO \quad (5)$$

These reactions resulting in a CO gas evolution are responsible for the increased porosity inside the CGN fibre and in the thick, defective oxidation layer on the surface of the Hi-Nicalon fibres during the creep process in air. It is suspected that this oxidation layer has been at least partially responsible for the scatter in the data for the stress exponent, n.

Recent results on the creep behaviour of CGN fibres in argon have shown that a rheological model quite accurately describes creep of Si–C–O fibres undergoing microstructural changes [9, 14, 20]. The decomposition of the CGN fibre in air and argon, which results in a decrease of the $SiO_xC_{1-(x/2)}$ volume fraction (weight loss) and an increase in solid volume fraction (grain growth) with time, was considered to cause an increase in fibre viscosity, therefore a continuous decrease in creep rate during the entire fibre life.

Hi-Nicalon fibres have greater creep resistance (about one order of magnitude) and higher thermal stability than do the CGN fibres. TEM analyses indicated that the structure of Hi-Nicalon fibres remained stable below ~ 1300 °C and a progressive growth of the SiC crystallites from 5 nm to 20–40 nm occurred with increasing temperature after annealing or creep above this temperature. The rate of crystallization was very rapid during creep at 1600 °C, (i.e. 0.1 h under an applied stress of 0.7 GPa). TEM observations revealed evidence that graphitization increases during heating in the Hi-Nicalon fibre, but not

TABLE IV Average SiC grain size as a function of the testing conditions

Atmosphere	T (°C)	σ_a (GPa)	t_f (h)	ε_f (%)	1 1 1 SiC grain size (nm)	
					Average	Maximum
As-received	–	–	–	–	5	10
Air	1280	0.70	41.3	2.44	10	25
	1400	0.45	30.9	4.49	10	20
	1400	0.70	25.3	8.41	20	40
Argon	1300	0.45	14.6	0.78	5	10
	1350	0.70	2.42	1.97	5	10
	1400	0.45	57.5	2.62	10	15
	1500	0.45	5.6	2.27	25	50
	1500	0.70	21.5	14.09	30	50
	1600	0.70	0.1	6.3	25	40
Annealed	1600	–	1	–	20	30

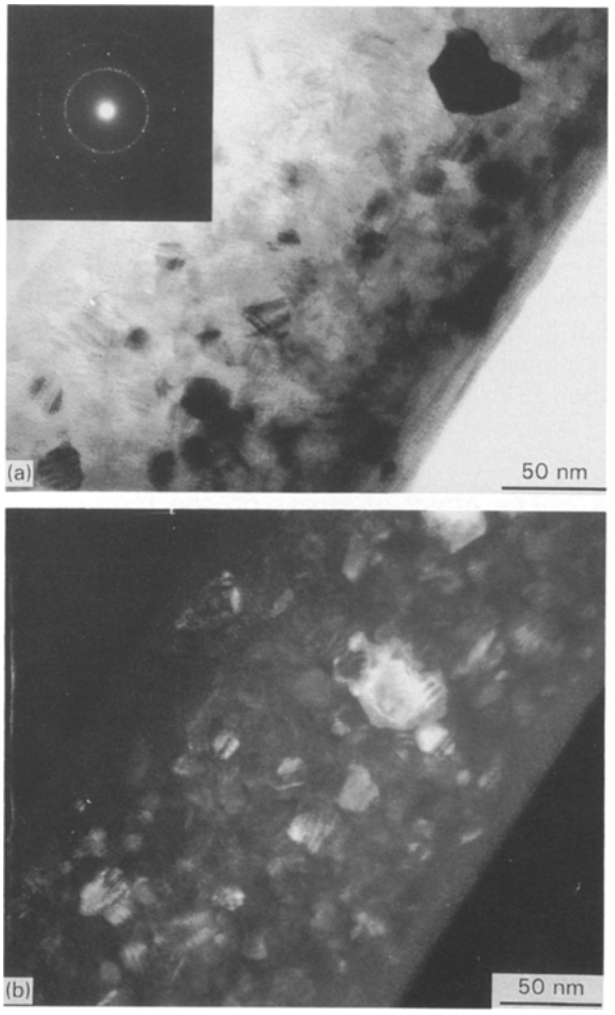

Figure 23 Longitudinal thin foil of the core of a fibre tested in argon at 1600 °C and 0.70 GPa for 0.1 h ($\varepsilon_f = 6.31\%$). (a) Bright-field micrograph and SAD pattern, (b) 1 1 1 SiC dark-field micrograph, showing grain growth.

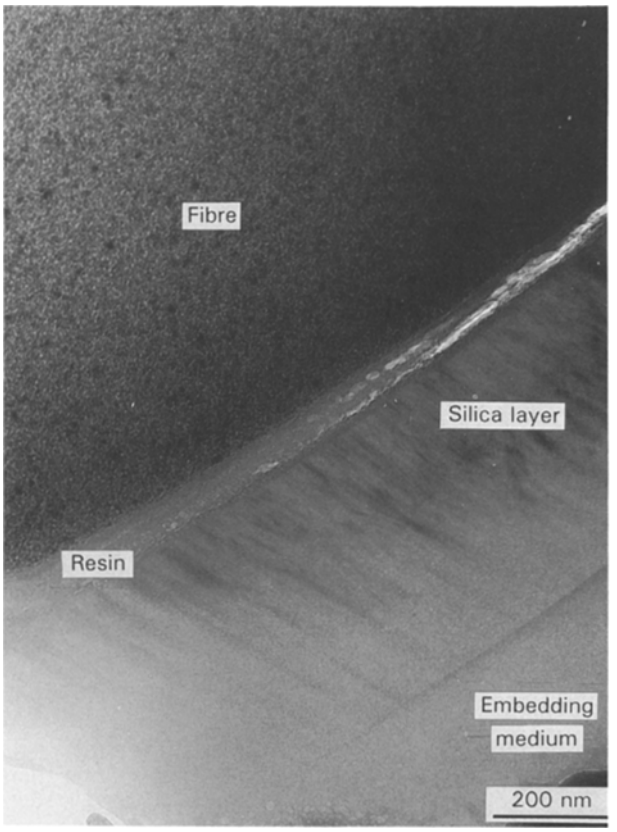

Figure 24 Bright-field image of the surface of a Hi-Nicalon fibre after creep in air at 1280 °C and 0.70 GPa for 41 h ($\varepsilon_f = 2.44\%$), showing the stable microstructure of the fibre surface and the debonding of the silica crust (the corresponding void being filled with the embedding resin).

as a result of the applied stress. Unstressed fibres along with creep specimens exhibited similar trends. The poorly organized carbon BSUs in the experimental fibre were seen to recrystallize after 1 and 10 h heat treatments at 1600 °C in argon and after creep exposure at 1400 °C in air ($t_f = 25.3$ h) and 1500 °C in argon ($t_f = 5.6$ and 21.5 h). Under the most severe testing conditions (i.e. $T = 1500$ °C and $\sigma_{app} = 0.70$ GPa), high creep strains were obtained (i.e. 14.09% in argon). Such a high strain resulted in a slight increase of the orientation of the carbon planes in the fibre axis direction. The SiC crystallization mechanism in Hi-Nicalon is not yet clearly established, but it is possibly related to the diffusion of CO and SiO gaseous species (the fibre has 0.5 at % oxygen) which react with SiC and carbon.

As reported before, nearly 90% of the fibres used in creep tests in argon failed after a very short period of

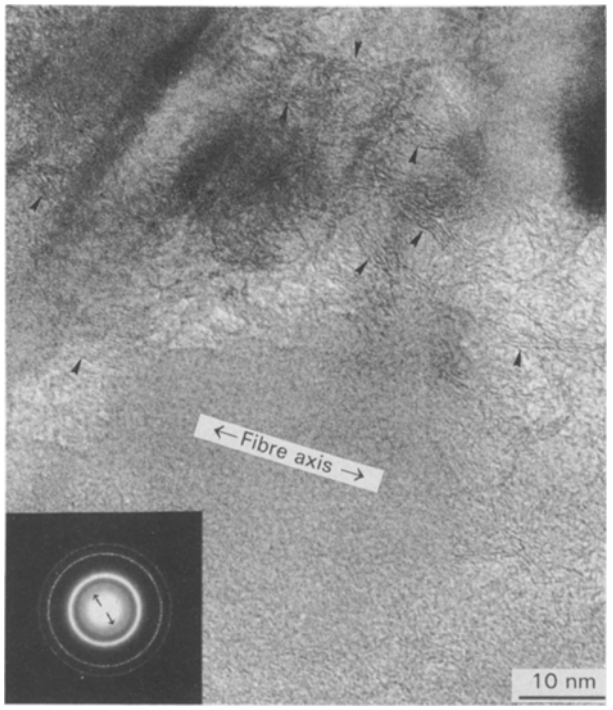

Figure 25 Lattice fringe imaging of a longitudinal thin foil of a fibre tested in argon at 1500 °C and 0.70 GPa for 21.5 h ($\varepsilon_f = 14.09\%$) showing the preferential orientation of the carbon layers in the loading direction. The SAD pattern in the inset exhibits two faint and diffuse 0 0 2 carbon arcs, as indicated by arrows.

time, and AES analyses indicated that many of these fibres had a carbon-rich layer on their surface. The inconsistencies in the time-to-failure values in argon may result from the variations of the rate of reaction for the active oxidation of SiC caused by varying amounts of oxygen from the environment and/or from the fibre.

4.2 Mechanism for creep

The apparent activation energies for creep of Hi-Nicalon in air (i.e. 345–423 kJ mol^{-1}) are higher than those calculated from argon experiments (193–292 kJ mol^{-1}). Because most of the oxidation layers were found to have thicknesses lower than 1 μm, it is believed that the reaction of the fibre with the environment and the formation of a viscous layer on the fibre surface in air did not affect the creep behaviour of the fibre. On the other hand, the lack of data for steady-state creep in argon precludes confirmation of these energies. Based on the TEM observations, the Hi-Nicalon fibre was considered as being a mixture of wrinkled carbon-layer packets and SiC grains. In this particular case, possible controlling creep mechanisms can be regarded as SiC grain-boundary sliding, carbon diffusion, and "dewrinkling" and sliding of carbon "crystallites". Comparing the literature values for the self-diffusion, E_{ld}, and grain-boundary diffusion, E_{gbd}, energies in SiC materials of either silicon, $E_{ld} = 912 \pm 5$ kJ mol^{-1}, $E_{gbd} = 564 \pm 9$ kJ mol^{-1}, or carbon, $E_{gbd} = 841 \pm 14$ kJ mol^{-1} [26], one finds little agreement with the calculated values of apparent activation energies for creep of Hi-Nicalon. Much higher apparent activation energies are also expected for carbon atoms in pyrolytic graphite (i.e. ~ 1045 kJ mol^{-1}), a mechanism controlled by the vacancy migration [27]. Other reported mechanisms for creep of graphite at low strains (i.e. < 10%–15%) and in various unimpregnated carbon yarns at $T > 2000$ °C, are dewrinkling of initially wrinkled graphitic sheet structures, and shear deformation along the basal plane, both of which are related to increases in preferred orientation in the material [28–29]. Activation energies for rayon and mesophase pitch-based fibres (WCA and P55, Amoco) were reported to be ~ 455 and 276 kJ mol^{-1}, respectively [30], which are close to the values of the apparent activation energies for creep of Hi-Nicalon fibres.

The calculated values for the stress exponent, n, were found to fall in the 2–3 range. Comparisons between these values and available data for creep of graphite are difficult, because of the different range of temperatures investigated. Most of the stress exponents reported for graphite were determined above 2000 °C and fall in the 6–8 range, which is much higher than the 2–3 range determined here. On the other hand, one finds a better correlation with values reported in the literature for the creep of a pitch-based carbon fibres (E 130) which exhibit ultra plastic creep strain ($\varepsilon_f = 38\%$) at ~ 2300 °C. The literature values fall in the 1–2 range which is close to the range determined in the present study (i.e. $n = 1.8$–2.0 in air from 1330–1400 °C and 2 in argon at 1400 °C) [31].

4.3. The effect of stress on the long-range ordering of the carbon structure

Very long chains of stacked carbon layers rapidly developed in samples that were creep tested at 1600 °C and 0.7 GPa. Natural anthracite, which is characterized by elongated (10–20 nm) pores and by pore walls composed of stacks of carbon BSUs (1–5 nm thick and up to 10 nm long), has been reported to graphitize at low temperatures (~ 600 °C) during axial compression experiments at 0.5 GPa (> 15% axial shortening) [32]. TEM examinations of deformed samples indicated that pores had coalesced and became aligned in the flattering plane of the experiments. Furthermore, the carbon BSUs became more ordered, with the eventual production of graphite. A strong preferred orientation of the 0 0 2 lattice fringes of carbon in the flattering plane was indeed observed. The activation energy for creep of natural anthracite was ~ 290 kJ mol^{-1}, which is in contrast with the thermally activated process for production of graphite from simple heating under ambient pressure ($Q \approx 1000$ kJ mol^{-1}).

4.4. Fibre necking

Significant necking of filaments occurred at high temperatures during creep, indicating high levels of local deformation. Reduction in diameter by a factor of 2 or more was sometimes observed. The experimental

Hi-Nicalon fibre was found to have a non-circular cross-section and a diameter variable along the fibre axis. Additionally, large processing defects were found in the fracture surface of some fibres. Commercial and experimental PCS-derived fibres have been reported to contain a considerable porosity at the nanometre scale [10, 11]. All theses features certainly lead to greater localized stresses during creep. This stress enhancement further affects the directional orientation of the long carbon chains developing at high temperatures. Taking into account the highly cross-linked structure of the carbon layers, all these effects may result in substantial deformations and consequently in fibre necking. Significant fibre necking, by a factor of 3 or more, has also been reported in the case of dry and carbon-impregnated bundles of rayon and pitch-based carbon fibres which had been subjected to creep above 2000 °C and stressed at 0.014–0.07 GPa [29].

5. Conclusions

The data reported and discussed on the creep behaviour of small-diameter polycrystalline SiC and Si–C–O fibres lead to the conclusion that the experimental Hi-Nicalon SiC fibres with a low oxygen content (O wt% < 0.4) have greater creep resistance (about one order of magnitude) under comparable conditions than do the commercial Si–C–O Nicalon fibres. The low oxygen-content SiC fibres also have superior rupture properties at room temperature. However, these fibres when subjected to creep show ultra plastic, localized deformations at 1400 °C in air under high stress levels. Significant deformations are also observed in argon at 1500 °C (i.e. 14%). Based on the values of the stress exponents and the apparent activation energies for creep, the processes involving dewrinkling of initially wrinkled carbon-layer packets into a position more nearly aligned with the tensile axis, sliding of these graphitic sheet structures, and collapse of fibre pores have been proposed for the creep mechanism of the Hi-Nicalon fibres.

There is, however, a need for more creep data and microstructural studies to correlate creep-rupture properties to microstructure and to confirm the proposed mechanisms of creep and rupture.

Acknowledgements

The authors acknowledge the French Ministry of Research and Société Européenne de Propulsion for their financial support of this project. The authors thank M. Lahaye for the AES analyses and M. Chambon for the TEM analyses, as well as R. Pailler and G. Chollon for their valuable suggestions concerning the thermomechanical stablity of the Hi-Nicalon fibre.

References

1. S. YAJIMA, J. HAYASHI and M. OMORI, *Chem. Lett.* **9** (1975) 931.
2. *Idem, ibid.* **10** (1976) 551.
3. R. W. RICE, *Ceram. Bull.* **62** (1983) 889.
4. R. R. WILLS, R. A. MARKLE and S. P. MUKHERJEE, *ibid.* **62** (1983) 904.
5. C. L. SCHILLING Jr, J. P. WESSON and T. C. WILLIAMS, *ibid.* **62** (1983) 912.
6. B. E. WALKER, *ibid.* **62** (1983) 916.
7. L. PORTE and A. SARTRE, *J. Mater. Sci.* **24** (1989) 271.
8. C. LAFFON, A. M. FLANK, P. LAGARDE, M. LARIDJANI, R. HAGEGE, P. OLRY, J. COTTERET, J. DIXMIER, L. MIQUEL, H. HOMMEL and A. P. LEGRAND, *ibid.* **24** (1989) 1503.
9. R. BODET, J. LAMON, N. JIA and R. E. TRESSLER, *J. Am. Ceram. Soc.*, in press.
10. M. H. JASKOWIAK and J. A. DICARLO, *ibid.* **72** (1989) 192.
11. R. BODET, N. JIA and R. E. TRESSLER, *J. Eur. Ceram. Soc.*, in press.
12. *Idem, ibid.*
13. G. SIMON and A. R. BUNSELL, *J. Mater. Sci.* **19** (1984) 3658.
14. N. JIA, R. BODET and R. E. TRESSLER, *J. Am. Ceram. Soc.*, in press.
15. K. OKAMURA, *Composites* **18** (1987) 107.
16. G. CHOLLON, M. CZERNIAK, R. PAILLER, X. BOURRAT and R. NASLAIN, in "Proceedings of the International Conference on High Temperature Ceramic Matrix Composites", edited by R. Naslain, J. Lamon and D. Doumeingt, ECCM-6, 20–24 September 1993, Bordeaux, France (Woodhead, Cambridge, 1993) pp. 109–116.
17. J. F. VILLENEUVE, D. MOCAER, R. PAILLER, R. NASLAIN and P. OLRY, *J. Mater. Sci.* **28** (1993) 1227.
18. J. F. VILLENEUVE and R. NASLAIN, *Compos. Sci. Technol.*, in press.
19. D. J. PYSHER, PhD thesis, Pennsylvania State University (1992).
20. N. JIA, PhD thesis, Pennysylvania State University (1993).
21. D. J. PYSHER, K. C. GORETTA, R. S. HODDER Jr and R. E. TRESSLER, *J. Am. Ceram. Soc.* **72** (1989) 284.
22. M. TAKEDA, Y. IMAI, H. ICHIKAWA, T. ISHIKAWA, N. KASAI, T. SUGUCHI and K. OKAMURA, *Ceram. Eng. Sci. Proc.* **13** (1993) 209.
23. E. GUGEL, in "Ceramics in Advanced Energy Technologies", Proceedings of the European Colloqium, Pette, Netherlands, 20–22 September 1982, Edited by H. Kröckel, M. Merz and O. Van der Biest (Reidel, Dordrecht, 1984) pp. 23–50.
24. W. R. CANNON and T. G. LANGDON, *J. Mater. Sci.* **18** (1983) 1.
25. Y. HASEGAWA, *Compos. Sci. Technol.* **37** (1990) 37.
26. J. A. DICARLO, *J. Mater. Sci.* **21** (1986) 217.
27. W. V. KOTLENSKY, *Carbon* **4** (1966) 209.
28. W. V. KOTLENSKY and H. E. MARTENS, in "Proceedings of the Fifth Conference on Carbon", Vol. 2, 1963, Pennsylvania State University, USA (Pergamon, New York, 1963) pp. 625–38.
29. L. A. FELDMAN, Aerospace Report No. ATR-88 (3728-02)-2 (The Aerospace Corporation, El Segundo, CA, 1988).
30. L. A. FELDMAN, in "Proceedings of the 16th Conference on Carbon", San Diego, (American Carbon Society, 1983) pp. 499–500.
31. K. KOGURE, J. G. LAVIN and G. SINES, "Extended Abstract of the 21st Conference on Carbon", Buffalo (American Carbon Society, 1993) pp. 16–17.
32. J. V. ROSS and R. M. BUSTIN, *Nature* **343** (1990) 58.

Received 15 February
and accepted 16 May 1994